

# INFUSING KNOWN OPERATORS IN CONVOLUTIONAL NEURAL NETWORKS FOR LATERAL STRAIN IMAGING IN ULTRASOUND ELASTOGRAPHY

Ali K. Z. Tehrani<sup>1</sup>, and Hassan Rivaz<sup>1</sup>

<sup>1</sup>Department of Electrical and Computer Engineering, Concordia University, Canada.

## ABSTRACT

Convolutional Neural Networks (CNN) have been employed for displacement estimation in ultrasound elastography (USE). High-quality axial strains (derivative of the axial displacement in the axial direction) can be estimated by the proposed networks. In contrast to axial strain, lateral strain, which is highly required in Poisson's ratio imaging and elasticity reconstruction, has a poor quality. The main causes include low sampling frequency, limited motion, and lack of phase information in the lateral direction. Recently, physically inspired constraint in unsupervised regularized elastography (PICTURE) has been proposed. This method took into account the range of the feasible lateral strain defined by the rules of physics of motion and employed a regularization strategy to improve the lateral strains. Despite the substantial improvement, the regularization was only applied during the training; hence it did not guarantee during the test that the lateral strain is within the feasible range. Furthermore, only the feasible range was employed, other constraints such as incompressibility were not investigated. In this paper, we address these two issues and propose kPICTURE in which two iterative algorithms were infused into the network architecture in the form of known operators to ensure the lateral strain is within the feasible range and impose incompressibility during the test phase.

**Index Terms**— Ultrasound Elastography, Convolutional Neural Networks, Physically inspired constraint, Known operator, Poisson's ratio

## 1. INTRODUCTION

Ultrasound Elastography (USE) provides information related to the stiffness of the tissue. Ultrasound (US) images before and after the tissue deformation (which can be caused by an external or internal force) are collected and compared to calculate the displacement map, indicating each individual sample's relative motion. The strain is computed by taking the derivative of the displacements. In free-hand palpation, the force is external and applied by the operator using the probe [1].

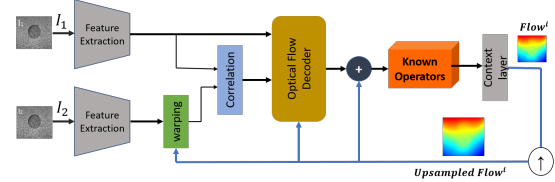


**Fig. 1.** MPWC-Net++ architecture with known operators. The network is iterative with 5 pyramid levels. The known operators refine the lateral displacement in each pyramid level to provide improved lateral displacement to the next pyramid level.

Convolutional Neural Networks (CNN) have been successfully employed for USE displacement estimation [2]. Unsupervised and semi-supervised training methods have been proposed, which enable the networks to use real US images for training [3, 4]. The proposed networks have achieved high-quality axial strains (derivative of the axial displacement in the axial direction). In contrast to axial strain, lateral strain, which is highly required in Poisson's ratio imaging and elasticity reconstruction, has poor quality due to the low sampling frequency and limited motion in the lateral direction.

Recently, physically inspired constraint in unsupervised regularized elastography (PICTURE) has been proposed [5]. This method aimed to improve lateral displacement by exploiting the high-quality axial displacement and the relation between the lateral and axial strains defined by the physics of motion.

Known operators have been widely utilized in deep neural networks. The basic idea is that some known operations (for example inversion of a matrix) are embedded inside the networks to simplify the training. The known operator can be viewed as the prior knowledge related to the physics of the problem. Maier *et al.* investigated the known operators in different applications such as computed tomography, magnetic resonance imaging, and vessel segmentation, and showed substantial reduction in the maximum error bounds [6].

In this paper, we aim to embed two algorithms in the CNNs to improve the lateral strains. The first algorithm limits the range of Effective Poisson's Ratio (EPR) inside the feasible range during the test time. It is important to note

that in contrast to our recent work [5], the EPR range is enforced using the regularization during the training phase and the known operators framework during the test phase; therefore, it is enforced during both training and test phases. The second algorithm aims to refine lateral displacements in an iterative algorithm obtained from incompressibility constraint.

## 2. MATERIALS AND METHODS

### 2.1. PICTURE

Lets  $\varepsilon_x$  denotes axial ( $x = 1$ ), lateral ( $x = 2$ ), and out-of-plane ( $x = 3$ ) strains. Assuming linear elastic, isotropic, and homogeneous material, the lateral strain can be obtained from the axial strain and the Poisson's ratio by  $\varepsilon_2 = -\nu \times \varepsilon_1$ . Real tissues are inhomogeneous, and boundary conditions exist; therefore, the lateral strain cannot be directly obtained by the axial strain and the Poisson's ratio alone. In this condition, the Effective Poisson's ratio (EPR) which is defined as  $v_e = \frac{-\varepsilon_{22}}{\varepsilon_{11}}$  is introduced [7]. EPR is not equal to Poisson's ratio, but it has a similar range of Poisson's ratio, which is 0.2-0.5 [8]. In PICTURE, a regularization is defined to exploit this range and the out-of-range EPRs are penalized. The procedure is as follows [5]:

1- Detect out-of-range EPRs by:

$$M(i, j) = \begin{cases} 0 & v_{emin} < \tilde{v}_e(i, j) < v_{emax} \\ 1 & otherwise \end{cases} \quad (1)$$

where  $\tilde{v}_e$  is the EPR obtained from the estimated displacements.  $v_{emin}$  and  $v_{emax}$  are two hyperparameters that specify the minimum and maximum accepted EPR values, which are assumed to be 0.1 and 0.6, respectively.

2- Penalize the out-of-range lateral strains using:

$$L_{vd} = |M \otimes (\varepsilon_{22} + \langle \tilde{v}_e \rangle \times \mathbf{S}(\varepsilon_{11}))|_2 \quad (2)$$

where  $\langle \tilde{v}_e \rangle$  is the average of EPR values within the feasible range. The operator  $\mathbf{S}$  denotes stop gradient operation, which is employed to avoid the axial strain being affected by this regularization.

3- Smoothness of EPR is also added by:

$$L_{vs} = \left| \frac{\partial v_e}{\partial a} \right|_1 + \beta \times \left| \frac{\partial v_e}{\partial l} \right|_1 \quad (3)$$

4- Picture loss is defined as  $L_V = L_{vd} + \lambda_{vs} \times L_{vs}$ , where  $\lambda_{vs}$  is the wight of the smoothness loss.

PICTURE loss is added to the data and smoothness losses of unsupervised training. It should be noted that during the training, the known operators are not utilized, and they are only employed for the test phase.

### 2.2. Known Operators

The training is performed without the known operators due to the high computational complexity of unsupervised training.

The known operators are added to the network in evaluation mode. We employed two known operators to impose physically known constraints on the lateral displacement.

The first known operator (we refer to it as Poisson's ratio clipper) limits the EPR to the feasible range of  $v_{emin} - v_{emax}$ . Although PICTURE tries to move all EPR values to the feasible range, in [5], it was shown that some samples in test time were still outside of the feasible range. Poisson's ratio clipper is an iterative algorithm since the lateral strains are altered by clipping the EPR values and affecting the neighbor samples' strain values. It should be mentioned that Poisson's ratio clipper does not visually improve the lateral strains substantially since PICTURE has already enhanced the lateral strain and Poisson's ratio clipper only limits a few remaining EPR values outside the feasible range.

The second algorithm employs the incompressibility of the tissue which can be formulated by:

$$\varepsilon_1 + \varepsilon_2 + \varepsilon_3 = 0 \quad (4)$$

in free-hand palpation the force is approximately uniaxial ( $\varepsilon_3 \simeq \varepsilon_2$ ); therefore the incompressibility can be written as:

$$\varepsilon_1 + 2 \times \varepsilon_2 = 0 \quad (5)$$

Guo *et al.* enforced incompressibility in an iterative algorithm [9]. We made a few changes to increase the method's robustness by adding Gaussian filtering in each iteration. The known operators are shown in Algorithm 1 and 2.

---

#### Algorithm 1: Poisson's ratio clipper

---

**input** : Lateral displacement  $w_l$ , Axial displacement  $w_a$ ,  $v_{emin}, v_{emax}, iteration$

**output**: Refined lateral displacement  $w_{ref}$

```

1  $w_{ref} \leftarrow w_l$  for  $q \leftarrow 1$  to  $iteration$  do
2    $e_{22} \leftarrow \frac{\partial w_l}{\partial l}$  // gradient in lateral direction.
3    $e_{11} \leftarrow \frac{\partial w_a}{\partial a}$  // gradient in axial direction.
4    $epr \leftarrow \frac{-e_{22}}{e_{11}}$ 
5    $epr(epr < v_{emin}) \leftarrow v_{emin}$  // Clip epr less than  $v_{emin}$ 
6    $epr(epr > v_{emax}) \leftarrow v_{emax}$  // Clip epr less than  $v_{emax}$ 
7    $w_{ref}(:, 2 \text{ to } end) \leftarrow w_{ref}(:, 1 \text{ to } end - 1) + epr \times e_{11}$ 
   // use the displacement of previous line and the clipped epr to
   find the displacement of the next line

```

---

### 2.3. Dataset and Quantitative Metrics

Data is collected from a breast phantom (Model 059, CIRS: Tissue Simulation & Phantom Technology, Norfolk, VA) using an Alpinion E-Cube R12 research US machine (Bothell, WA, USA). The center frequency was 8 MHz and the sampling frequency was 40 MHz. The Young's modulus of the experimental phantom was 20 kPa and contains several inclusions with Young's modulus of higher than

---

**Algorithm 2:** Guo *et al.* refinement
 

---

**input :** Lateral displacement  $w_l$ , Axial displacement  $w_a$  of size  $w \times h$ , *iteration*,  $\lambda_1$ ,  $\lambda_2$

**output:** Refined lateral displacement  $w_{ref}$

```

1  $w_{ref} \leftarrow w_l$  for  $q \leftarrow 1$  to iteration do
2   for  $i, j$  in  $w, h$  do
3      $\delta = W_l(i, j - 1) - 2W_l(i, j) + W_l(i, j + 1) +$ 
        $W_a(i + 1, j + 1) - W_a(i - 1, j) - W_a(i, j -$ 
        $1) + W_a(i - 1, j - 1) + \lambda_1(W_{ref}^{q-1} - W_{ref}^{q-2})$ 
4      $w_{ref}^q = \text{Gauss}(w_{ref}^{q-1} + \lambda_2 \times \delta)$  // Gaussian
       filtering to reduce noise
  
```

---

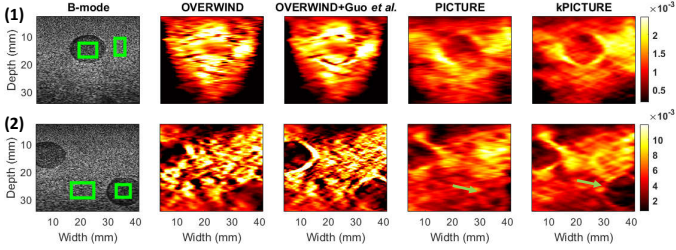


**Fig. 2.** The experimental phantom lateral strains obtained by the evaluated methods. The target and background windows for calculation of CNR and SR are marked in the B-mode images. The samples 1 and 2 are taken from different locations of the tissue-mimicking breast phantom.

40 kPa. This data was publicly made available online at <http://code.sonography.ai> in [10].

Two well known metrics of Contrast to Noise Ratio (CNR) and Strain Ratio (SR) are utilized to evaluate the compared methods. Two Regions of Interest (ROI) are selected to compute these metrics and they can be defined as [1]:

$$CNR = \sqrt{\frac{2(\bar{s}_b - \bar{s}_t)^2}{\sigma_b^2 + \sigma_t^2}}, \quad SR = \frac{\bar{s}_t}{\bar{s}_b}, \quad (6)$$

where the subscript  $t$  and  $b$  denote the target and background ROIs. The SR is only sensitive to the mean ( $\bar{s}_X$ ), while CNR depends on both the mean and the standard deviation ( $\sigma_X$ ) of ROIs. For stiff inclusions as the target, higher CNR correlates with better quality strain, and lower SR translates to a higher difference between the target and background strains.

#### 2.4. Network architecture and training

We employed MPWC-Net++ [11]. The network architecture is shown in Fig. 1. The training schedule is similar to [5], known operators are not present in the training and only employed during the test.

**Table 1.** Quantitative Results

	sample (1)		sample (2)	
	CNR	SR	CNR	SR
OVERWIND	1.94 ± 1.16	0.678 ± 0.147	2.31 ± 1.57	0.515 ± 0.195
OVERWIND + Guo <i>et al.</i>	2.26 ± 1.32	0.647 ± 0.144	1.80 ± 0.85	0.518 ± 0.166
PICTURE	9.63 ± 2.80	<b>0.432 ± 0.072</b>	1.14 ± 0.62	0.845 ± 0.122
kPICTURE	<b>11.48 ± 2.65</b>	0.499 ± 0.053	<b>6.32 ± 0.29</b>	<b>0.298 ± 0.080</b>

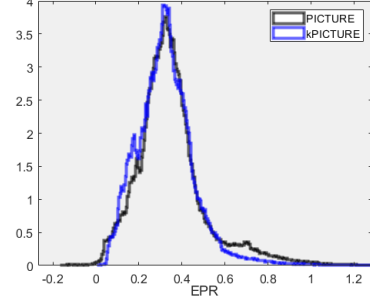


**Fig. 3.** The histogram for the results (experimental phantom sample 2) with known operator has successfully limited the EPR range.

### 3. RESULTS

#### 3.1. Compared methods

The evaluated methods are:

- Total Variation Regularization and Window-based time delay estimation (OVERWIND) is an optimization-based method that utilizes windowing and total variation in the optimization cost function [12].
- The post-processing method of Guo *et al.* which employs the output of OVERWIND as the initial displacement (OVERWIND+ Guo *et al.*).
- Our recent work PICTURE which penalize EPR values outside of feasible range [5].
- The proposed method named kPICTURE which has PICTURE trained weights and added the known operators.

#### 3.2. Experimental phantom results

The experimental phantom lateral strains of two samples taken from different locations of the tissue-mimicking breast phantom are depicted in Fig. 4, and the quantitative results are given in Table 1. Visual inspection of Fig. 4 denotes that Guo *et al.* outperforms OVERWIND, and the strain images obtained by kPICTURE have a higher quality than those of PICTURE. Furthermore, kPICTURE has the highest quality strain images among the compared methods. For example, the inclusion marked by the arrow is clearly visible in kPICTURE, while it is not in PICTURE and OVERWIND due to over-smoothing and is barely visible in OVERWIND+Guo *et al.*

Quantitative results also show that kPICTURE has the highest CNR values. The high CNR and low SR for sample 2 indicate that the bottom inclusion (target window is selected within this inclusion) is detected by kPICTURE. In contrast, low CNR and high SR of other methods show that this inclusion is not visible in the strain images obtained by the other methods.

The histograms of EPR values of PICTURE and kPICTURE are illustrated for the experimental phantom sample (2). Although PICTURE limits the range of EPR using a regularization (Eq 2), some EPR values are outside the feasible range. kPICTURE further limits the EPR values; only a small number of samples are outside the physically correct range.

#### 4. CONCLUSION

In this paper, we incorporated two known operators inside a network, which is trained by physically inspired constraint, specifically for lateral strain imaging. The proposed operators provide a refinement in each pyramid level of the architecture and substantially improve the lateral strain image quality.

#### 5. COMPLIANCE WITH ETHICAL STANDARDS

This is an experimental phantom study for which no ethical approval was required.

#### 6. ACKNOWLEDGMENTS

We acknowledge the support of the Natural Sciences and Engineering Research Council of Canada (NSERC).

#### 7. REFERENCES

- [1] Jonathan Ophir, S Kaisar Alam, Brian Garra, F Kallel, E Konofagou, T Krouskop, and T Varghese, “Elastography: ultrasonic estimation and imaging of the elastic properties of tissues,” *Proceedings of the Institution of Mechanical Engineers, Part H: Journal of Engineering in Medicine*, vol. 213, no. 3, pp. 203–233, 1999.
- [2] Ali KZ Tehrani and Hassan Rivaz, “Displacement estimation in ultrasound elastography using pyramidal convolutional neural network,” *IEEE transactions on ultrasonics, ferroelectrics, and frequency control*, vol. 67, no. 12, pp. 2629–2639, 2020.
- [3] Ali KZ Tehrani, Morteza Mirzaei, and Hassan Rivaz, “Semi-supervised training of optical flow convolutional neural networks in ultrasound elastography,” in *International Conference on Medical Image Computing and Computer-Assisted Intervention*. Springer, 2020, pp. 504–513.
- [4] Rémi Delaunay, Yipeng Hu, and Tom Vercauteren, “An unsupervised approach to ultrasound elastography with end-to-end strain regularisation,” in *International Conference on Medical Image Computing and Computer-Assisted Intervention*. Springer, 2020, pp. 573–582.
- [5] Ali KZ Tehrani and Hassan Rivaz, “Physically inspired constraint for unsupervised regularized ultrasound elastography,” in *International Conference on Medical Image Computing and Computer-Assisted Intervention*. Springer, 2022, pp. 218–227.
- [6] Andreas K Maier, Christopher Syben, Bernhard Stimpel, Tobias Würfl, Mathis Hoffmann, Frank Schebesch, Weilin Fu, Leonid Mill, Lasse Kling, and Silke Christiansen, “Learning with known operators reduces maximum error bounds,” *Nature machine intelligence*, vol. 1, no. 8, pp. 373–380, 2019.
- [7] Lifeng Ma and Alexander M Korsunsky, “The principle of equivalent eigenstrain for inhomogeneous inclusion problems,” *International Journal of Solids and Structures*, vol. 51, no. 25-26, pp. 4477–4484, 2014.
- [8] PH Mott and CM Roland, “Limits to poisson’s ratio in isotropic materials—general result for arbitrary deformation,” *Physica Scripta*, vol. 87, no. 5, pp. 055404, 2013.
- [9] Li Guo, Yan Xu, Zhengfu Xu, and Jingfeng Jiang, “A pde-based regularization algorithm toward reducing speckle tracking noise: A feasibility study for ultrasound breast elastography,” *Ultrasonic imaging*, vol. 37, no. 4, pp. 277–293, 2015.
- [10] Ali KZ Tehrani, Mostafa Sharifzadeh, Emad Boctor, and Hassan Rivaz, “Bi-directional semi-supervised training of convolutional neural networks for ultrasound elastography displacement estimation,” *IEEE Transactions on Ultrasonics, Ferroelectrics, and Frequency Control*, 2022.
- [11] Ali K.Z. Tehrani and Hassan Rivaz, “Mpw-net++: evolution of optical flow pyramidal convolutional neural network for ultrasound elastography,” in *Medical Imaging 2021: Ultrasonic Imaging and Tomography*. International Society for Optics and Photonics, 2021, vol. 11602, p. 1160206.
- [12] M Mirzaei, A Asif, and H Rivaz, “Combining total variation regularization with window-based time delay estimation in ultrasound elastography,” *IEEE transactions on medical imaging*, 2019.